Oxidative stress activates red cell adhesion to laminin in sickle cell disease

Maria Alejandra Lizarralde-Iragorri, Sophie Lefevre, Sylvie Cochet, Sara El Hoss, Valentine Brousse, Anne Filipe, Michael Dussiot, Slim Azouzi, Caroline Le van Kim, Fernando Rodrigues-Lima, et al.

▶ **To cite this version:**

Maria Alejandra Lizarralde-Iragorri, Sophie Lefevre, Sylvie Cochet, Sara El Hoss, Valentine Brousse, et al.. Oxidative stress activates red cell adhesion to laminin in sickle cell disease. Haematologica, 2020, 106 (9), pp.haematol.2020.261586. 10.3324/haematol.2020.261586 . hal-02929195

HAL Id: hal-02929195
https://hal.science/hal-02929195

Submitted on 17 Sep 2020

HAL is a multi-disciplinary open access archive for the deposit and dissemination of scientific research documents, whether they are published or not. The documents may come from teaching and research institutions in France or abroad, or from public or private research centers.

L'archive ouverte pluridisciplinaire **HAL**, est destinée au dépôt et à la diffusion de documents scientifiques de niveau recherche, publiés ou non, émanant des établissements d'enseignement et de recherche français ou étrangers, des laboratoires publics ou privés.

Oxidative stress activates red cell adhesion to laminin in sickle cell disease

Maria Alejandra Lizarralde-Iragorri[1,2,3*], Sophie D. Lefevre[1,2,3*], Sylvie Cochet[1,2,3], Sara El Hoss[1,2,3], Valentine Brousse[1,2,3,4], Anne Filipe[1,2,3,5], Michael Dussiot[6], Slim Azouzi[1,2,3], Caroline Le Van Kim[1,2,3], Fernando Rodrigues-Lima[5], Olivier Français[7], Bruno Le Pioufle[8], Thomas Klei[9], Robin van Bruggen[9] and Wassim El Nemer[1,2,3#]

[1]Université de Paris, UMR_S1134, BIGR, Inserm, F-75015 Paris, France.

[2]Institut National de la Transfusion Sanguine, F-75015 Paris, France.

[3]Laboratoire d'Excellence GR-Ex, Paris, France.

[4]Service de Pédiatrie Générale et Maladies Infectieuses, Hôpital Universitaire Necker Enfants Malades, Paris, France.

[5]Université de Paris, BFA, UMR 8251, CNRS, F-75013 Paris, France

[6]Institut Imagine, INSERM U1163, CNRS UMR8254, Université Paris Descartes, Hôpital Necker Enfants Malades, 75015, Paris, France.

[7]ESYCOM, Univ Gustave Eiffel, CNRS UMR 9007, ESIEE Paris, F-77454 Marne-la-Vallee, France.

[8]Université Paris-Saclay, ENS Paris-Saclay, CNRS Institut d'Alembert, LUMIN, Gif sur Yvette, France.

[9]Dept. of Blood Cell Research, Sanquin Research and Lab Services and Landsteiner Laboratory, Academic Medical Center, University of Amsterdam, Amsterdam, The Netherlands.

*These authors contributed equally to this work.

Running title: Activation of SCD RBC adhesion by oxidative stress

#To whom correspondence should be addressed: Wassim El Nemer, Inserm, UMR_S1134, INTS, 6 rue Alexandre Cabanel, 75015 Paris, France, E-mail: wassim.el-nemer@inserm.fr; Phone: +33144493071; Fax: +33143065019.

Text word count: 4160
Abstract word count: 194
Number of figures: 5
Number of videos: 1
Number of references: 48

Acknowledgments

We thank Mr Mickaël Marin, Mr Harvey Nagy and Dr Jean-Philippe Semblat for technical support. The work was supported by the Institut National de la Santé et de la Recherche Médicale (Inserm), the Institut National de la Transfusion Sanguine, the Laboratory of Excellence GR-Ex, reference ANR-11-LABX-0051, and the Laboratory of Excellence LaSIPS (ANR-10-LABX-0040-Lasips). The labex GR-Ex is funded by the IdEx program "Investissements d'avenir" of the French National Research Agency, reference ANR-18-IDEX-0001. Maria Alejandra Lizarralde Iragorri and Sara El Hoss were funded by the Ministère de l'Enseignement Supérieur et de la Recherche (Ecole Doctorale BioSPC); they received financial support from: Club du Globule Rouge et du Fer and Société Française d'Hématologie.

Abstract

Vaso-occlusive crises are the hallmark of sickle cell disease (SCD). They are believed to occur in two steps, starting with adhesion of deformable low-dense red blood cells (RBCs), or other blood cells such as neutrophils, to the wall of post-capillary venules, followed by trapping of the denser RBCs or leukocytes in the areas of adhesion because of reduced effective lumen-diameter. In SCD, RBCs are heterogeneous in terms of density, shape, deformability and surface proteins, which accounts for the differences observed in their adhesion and resistance to shear stress. Sickle RBCs exhibit abnormal adhesion to laminin mediated by Lu/BCAM protein at their surface. This adhesion is triggered by Lu/BCAM phosphorylation in reticulocytes but such phosphorylation does not occur in mature dense RBCs despite firm adhesion to laminin. In this study, we investigated the adhesive properties of sickle RBC subpopulations and addressed the molecular mechanism responsible for the increased adhesion of dense RBCs to laminin in the absence of Lu/BCAM phosphorylation. We provide evidence for the implication of oxidative stress in post-translational modifications of Lu/BCAM that impact its distribution and *cis*-interaction with glycophorin C at the cell surface activating its adhesive function in sickle dense RBCs.

Introduction

Sickle cell disease (SCD) is an autosomal recessive disorder caused by a single mutation in the 6^{th} codon of the β globin gene resulting in the expression of an abnormal hemoglobin that polymerizes under hypoxic conditions driving red blood cell (RBC) sickling (1). SCD is a multisystem disease characterized by hemolytic anemia, recurrent painful vaso-occlusive crises (VOCs), stroke, acute chest syndrome, organ failure and high susceptibility to infections (2, 3). On the cellular level, SCD is characterized by dehydration and RBC sickling, which decrease cell deformability and increase rigidity resulting in altered blood rheology and microcirculatory flow (2-6). In addition, RBCs are known to be highly adhesive in SCD (7-9). This abnormal adhesion to the endothelium is a contributing factor of the VOCs and believed to be triggered by signaling cascades that activate adhesion proteins at the red cell surface (10). A two-step model, based on *in vivo* vaso-occlusion observations in SCD mouse models, postulates that adhesion of deformable low-dense RBCs and stress reticulocytes reduces effective lumen-diameter of post-capillary venules promoting selective trapping of the denser and misshapen RBCs in the areas of adhesion. However, random precapillary obstruction by a small number of dense RBCs also contributes to VOCs as well as the entrapment of leukocytes and platelets (11-14).

Sickle RBCs are very heterogeneous in terms of age, shape and surface proteins. These variabilities account for the differences observed in cell adhesion and resistance to shear stress under flow conditions (11). In SCD, among other proteins and mechanisms, adhesion proteins LW/ICAM-4 (Landsteiner-Wiener/intercellular adhesion molecule-4) and Lu/BCAM (Lutheran/basal cell adhesion molecule) are abnormally activated and believed to prime adhesion of RBCs to endothelial cells and/or subendothelial matrix proteins exposed to the bloodstream following vascular damage, contributing to microvasculature blockade (10, 15-21).

Lu/BCAM is an adhesion molecule with wide tissue distribution (22, 23). Lu/BCAM-mediated cell adhesion to laminin can be triggered either by the phosphorylation of its serine 621 (17, 24) or by the dissociation of its cytoplasmic domain from the spectrin-based skeleton (25, 26). In SCD, phosphorylation of Lu/BCAM was shown to occur in low-density (LD) RBCs (27), mainly reticulocytes, consistent with the adhesion of these cells to laminin (27, 28). However, despite firm adhesion to laminin of high-density (HD) RBCs, Lu/BCAM phosphorylation is very minor in this subpopulation and these cells do not respond to cAMP inducers such as forskolin (28). The mechanism underlying this increased adhesion is still unknown.

In this study, we investigated the molecular mechanism responsible for the increased adhesion of sickle HD RBCs to laminin. We provide evidence for the implication of oxidative stress in post-translational modifications of Lu/BCAM that impact its distribution and *cis*-interactions at the cell surface and activate its adhesive function.

Methods

Patients

The study was conducted in accordance with the Declaration of Helsinki and was approved by the Regional Ethics Committee (n°3215 CPP Ile de France III). Blood samples were recovered from blood tubes drawn for medical care at Necker Hospital (Paris) after written informed consent. Blood samples were collected on ethylenediaminetetraacetic acid (EDTA) from a total of 39 patients with sickle cell anemia (SS and Sbeta° genotypes) (females and males; median age: 8 years [Min-Max: 2-53 years]), and from 26 healthy donors [age range: 18-70, as per Etablissement Français du Sang (EFS) criteria]. Sickle patients were not on a regular transfusion program nor under Hydroxyurea (HU) treatment. All experiments were performed with fresh blood samples, within 2 hours after blood was drawn.

Percoll fractionation

RBC subpopulations were obtained from sickle whole blood fractionation as previously described (27), using a Percoll triple-density fractionation (densities: 1.076, 1.096, and 1.11). Three different density layers were obtained and collected as follows: LD (low density, rich in reticulocytes), D (dense), and HD (high density, rich in irreversibly sickled cells).

Microfluidic assays

The microfluidic filtering design is based on eight mechanical filtering units associated in parallel and connected together with a microchannel network. Each filtering unit is composed of 5 parallel rows comprising pillars of 15 μm diameter separated by slits of 10, 8, 7, 6 or 5 μm (Figure 1A) or 4 parallel rows with slits of 5, 4, 3 or 2 μm (Supplemental Figure S1). Side flow is rendered possible in the device, the U form filter zone comprises

pillars with a 5 μm gap between them. In order to reduce the hydraulic resistance of the full design, the microchannel network is 25 μm-high compared to the 5 μm height of each filtering unit (Figure 1A). The microfluidic device was made of polydimethylsiloxane (PDMS, Sylgard), a silicone elastomer (29), using standard microfabrication and molding. The mold was fabricated by the micro-patterning of two successive SU-8 photoresist layers (Microchem, Newton, MA) to obtain a two-levels negative mold on a 4 inches Silicon substrate. The SU8 layers thicknesses were 5 μm and 25 μm, corresponding respectively to the height of the filtering units and the microchannels network. A mixture of PDMS and curing agent was poured on the SU8 mold, and reticulated at 75°C for 2 h. Access through-holes were then punched, using biopsy punchers (diameter of 1.5 mm). The PDMS device, with open channels formed on one of its sides, was then assembled to a microscope coverslip, using O_2 plasma activation (30 W, 300 mT, 20 s) to achieve a covalent bonding. Luer (TM) connectors were then inserted at the inlet and outlet of this microfluidic device, to achieve the sample injection with the flow controller.

For each assay, 10 μl of RBC pellet were stained with either PKH67 fluorescent Cell Linker Kit (green) or PKH26 fluorescent Cell Linker Kit (red) according to the manufacturer's instructions (Sigma Aldrich). A 1% hematocrit solution in CellStab containing equal concentration of green and red stained RBCs were loaded in the input well of the chip and perfused at constant pressure (250 mBar) using an MFCS™-EZ-1C pump (Fluigent). RBC trapping within each filtering unit was monitored over time by sequential fluorescence images acquired using an inverted AxioObserver Z1 microscope coupled with a high resolution AxioCam MRm Rev.3 camera (Carl Zeiss). Green and red fluorescent RBCs were visualized using the 470 and 555 nm Colibri LED (Carl Zeiss), respectively. Images were then analyzed using ImageJ software (30).

Flow adhesion assays and RBC counting

RBC adhesion to Laminin 521 was evaluated under flow conditions using capillary flow chambers. Recombinant human Laminin 521 (BioLamina, Sundbyberg, Sweden) at 5 ng/µl was immobilized in Vena8 Endothelial+^{TM} biochips (internal channel dimensions: length 20 mm, width 0.8 mm, height 0.12 mm). RBCs were perfused at 5.10^7 RBCs/ml for 10 min at 0.5 dyn/cm^2 and 6 min washouts were performed at 1, 2, 3, 4, 5, 6, 7, 8, 9 and 10 dyn/cm^2 using the ExiGo^{TM} pump (Cellix Ltd, Dublin, Ireland). After each wash, images of adherent RBCs were taken using the AxioObserver Z1 microscope (10X objective) (Carl Zeiss, Le Pecq, France). Adherent RBCs were counted on each field using Image J.

The number of immobile RBCs was assessed by using the Image Calculator option of the Image J software (30). Picture of one area at 2 dyn/cm² was combined to the picture of the same area taken at 3 dyn/cm². On the newly created image, immobile cells appeared in dark grey whereas cells present on only one of the two combined images appeared in light grey. Dark grey object were counted with Image J software after setting an appropriate threshold.

Control blood sample oxidation

Control RBCs were washed with PBS 1X (Thermo Fisher), suspended at 20% hematocrit in either PBS or 270 µM Cumene Hydroperoxide (SIGMA-ALDRICH) and incubated for 2 hours with constant mild shaking. After incubation, RBC suspensions were centrifuged, the supernatant was discarded and the RBC pellets were used for subsequent experiments.

Confocal microscopy

Imaging was performed on the Confocal LSM 510 META-TIRF (Zeiss, Oberkochen, Germany). LASX software was used to set up and analyze the experiments (Leica microsystems, Wetzlar, Germany).

Imaging flow cytometry assays

Expression of Lu/BCAM on the RBC surface was analyzed using F241 mouse monoclonal antibody. After 1-hour incubation with F241 (d: 1/10), the secondary anti-mouse APC-conjugated antibody (d: 1/100) (Beckman Coulter) was added for 1 hour then RBCs were washed and suspended in 200 µl of thiazole orange (TO) dye (Retic-Count^{TM}, Becton-Dickinson) for 30 min to label reticulocytes. RBCs were analyzed using ImageStream®^{X} Mark II Imaging Flow Cytometer (Merck Millipore) (60X magnification) and the IDEAS software (version 6.2). Lu/BCAM-positive mature RBCs (Lu APC) were gated, excluding the reticulocytes (TO-positive events). Using the Modulation Feature, that measures the intensity range of an image, normalized between 0 and 1 (Formula: Modulation = Max Pixel - Min Pixel / Max Pixel + Min Pixel), reflecting the florescent signal distribution, we defined 2 subpopulations of mature Lu/BCAM RBCs: Low-Modulation (Spots) and High-Modulation (Patches). Based on the *x*-axis Modulation_M11_Ch11 APC and *y*-axis Mean Pixel_M11_Ch11 APC, the "Spots" population was between -0.039 and 0.231, and the "Patches" population was between 0.235 and 0.552.

Flow cytometry assays

Protein sialylation was measured by incubating RBC suspensions with biotinylated Lectin (35 ng/ml) (*Maackia amurens* Lectin II, VECTOR) for 1 hour with constant shaking. After washes, Streptavidin-488 (10 µg/ml) (Streptavidin Alexa Fluor 488 conjugate, Invitrogen) was added to the pellet, and incubated for 30 min in the dark. GPC sialylation on

mature RBCs was determined by incubating the RBC suspensions with the anti-BRIC 4 (d: 1/100) antibody or anti-BRIC 10 (d: 1/200) antibody (IBGRL Research Products). After 1 hour incubation at room temperature and several washes, the RBC pellet was incubated with the secondary anti-mouse APC antibody (d: 1/100) (Beckman Coulter) for 45 min in the dark. RBCs were analyzed using a BD FACS Canto II (BD Biosciences), the data obtained was analyzed using the FCS Express 6 software (De Novo).

Statistical analyses

Data was analyzed by two-tailed Mann-Whitney or Wilcoxon test, and Paired *t* test using the GraphPad Prism 7.00 software. *P ≤ 0.05, **P ≤ 0.01, ***P ≤ 0.001 and ****P ≤ 0.0001 were considered significant.

Results

Validating HD and LD RBC isolation

Deformability of AA and SS RBCs

HD RBCs are known to be rigid cells with reduced deformability, which contributes to capillary blockade *in vivo*. To validate the fractionation method used to isolate LD and HD RBCs from SCD blood samples, we assessed their deformability after isolation at the single cell level using a microfluidic approach based on perfusing RBCs in a spleen-like biomimetic chip with filtering units comprising slits from 5 down to 2 µm (31) (Supplemental Figure S1). First, we analyzed the deformability of total RBCs using this biochip. AA and SS RBCs were fluorescently labeled with PKH26 (red) and PKH67 (green), respectively, and mixed in 1:1 ratio into a suspension at 0.1% hematocrit. Perfusing this RBC suspension led to a total blockade of the biochip indicating that the slit dimensions were not suitable for testing deformability of SS RBCs. As the blockade occurred at the 5 µm wall we designed a new biochip with slit dimensions of 10 to 5 µm (Figure 1A). Perfusing the 1:1 AA-SS RBC suspension into this biochip showed preferential trapping of SS RBCs (Figure 1B), with these cells showing a higher retention rate than AA RBCs (Figure 1C), indicating that the biochip was a good tool to assess RBC deformability in the SCD context.

Deformability of LD and HD sickle RBCs

RBC suspensions were prepared with PKH67-labeled LD RBCs and PKH26-labeled HD RBCs (1:1) and perfused in the biochip. Both LD and HD RBCs were retained in the biochip, mainly at the 5 µm wall, indicating the presence of rigid cells in both populations (Figure 1D). Quantification of both RBC types retained in the 5 µm peripheral slits showed more HD than LD RBCs (Figure 1E) indicating that RBCs from the HD fraction were less deformable than those from the LD fraction, thus validating our fractionation method based on cell density.

HD RBCs are more resistant to shear stress and adhere more firmly to laminin than LD RBCs

RBC adhesion to laminin under flow conditions

We assessed the adhesive properties and resistance to shear stress of RBC sub-populations by performing adhesion assays under flow conditions with LD and HD RBCs from 7 SCD patients using channels coated with laminin 521. Both RBC types showed significant adhesion to laminin but there was a difference between them regarding resistance to shear stress. This resistance was first assessed by calculating the percentage of cells adhering at a given shear stress considering the number of adhering cells at 1 dyn/cm² as 100%. HD RBCs were more resistant than LD RBCs at physiological shear stresses for capillaries or post-capillary venules (2 to 5 dyn/cm²), while at high shear stress (10 dyn/cm²) both cell types showed no significant difference (Figure 2A). Exploring the cellular dynamics, we observed that LD RBCs comprised a higher proportion of rolling cells than HD RBCs (video 1), with a higher proportion of mobile cells covering a greater distance within the same time frame (Figure 2B). We assessed cell dynamics by determining the percentage of immobile cells between two consecutive shear stress steps. To do so, computational treatment of brightfield images of the same fields at two consecutive shear stresses was done to identify and count the cells that remained at the same spot between the two time-points (Figure 2C, supplemental Figure S2.A). The percentage of immobile cells was constantly higher for HD than LD RBCs (Figure 2D), indicating that HD RBCs were more firmly attached to laminin than LD RBCs even at high shear stress.

Lu/BCAM expression pattern on adherent LD and HD RBCs

To gain insight into the potential mechanism underlying this difference between LD and HD RBCs, cells were fixed after the 7 dyn/cm² step, stained fluorescently for Lu/BCAM and

analyzed by confocal microscopy. There was a difference in the expression pattern of Lu/BCAM between LD and HD RBCs at the interface with laminin. HD RBCs showed homogeneous distribution of Lu/BCAM with some cells showing intense staining and the presence of bigger spots suggestive of potential Lu/BCAM aggregates (Figure 2E, supplemental Figure S2.B). LD RBCs showed cells with smaller surface contact area, large fluorescent patches and very fine fluorescent membrane extensions tethering the cells to the surface (Figure 2E). The proportion of RBCs exhibiting membrane tethers was higher in LD (55.6%) than in HD RBCs (8.2%) (Figure 2F), and tethers were also longer in LD RBCs (Figure 2G) suggesting a more dynamic lipid bilayer in LD RBCs.

Oxidation activates AA RBC adhesion to laminin

We have previously shown that Lu/BCAM-mediated adhesion to laminin is activated by phosphorylation of serine 621 of its cytoplasmic tail (17). In SCD, this phosphorylation takes place in reticulocytes, with very low levels of phosphorylation detected in HD RBCs (27). Considering the high levels of adhesion of HD RBCs, we hypothesized that Lu/BCAM might be activated by post-translational modifications triggered by oxidative stress. To test this hypothesis, we assessed adhesion of control (AA) RBCs under oxidative conditions after incubation with Cumene Hydroperoxide (270 μM), an agent that induces membrane lipid peroxidation. AA RBCs showed the expected residual adhesion to laminin, that was significantly increased after incubation with Cumene Hydroperoxide (Figure 3A, supplemental Figure S3). This was not due to a difference in Lu/BCAM expression level between oxidative and control conditions as determined by flow cytometry measuring the percentage of Lu/BCAM-positive RBCs and their mean fluorescence intensity (MFI) (Figure 3B). Moreover, this increased adhesion was not due to increased phosphorylation of Lu/BCAM as determined by western-blot using an anti-phosphoSerine antibody (not shown).

Oxidative stress alters Lu/BCAM distribution at the red cell surface

Analysis of Lu/BCAM membrane distribution by confocal microscopy

We evaluated the impact of oxidation on the distribution of Lu/BCAM at the red cell surface using confocal microscopy. As expected and previously shown (26), Lu/BCAM showed a punctuated expression pattern at the red cell surface (Figure 4A left panel, supplemental Figure S4). Under oxidative conditions, there was more RBCs with large fluorescent patches suggestive of Lu/BCAM aggregation (Figure 4A right panel, supplemental Figure S4). To check if this was a general feature of membrane proteins under oxidative conditions we stained for ICAM-4, another member of the immunoglobulin superfamily, and found no difference in its membrane distribution between both conditions (Figure 4B) indicating that oxidation targets Lu/BCAM membrane distribution through a specific mechanism.

Analysis of Lu/BCAM membrane distribution by imaging flow cytometry

We assessed Lu/BCAM membrane distribution using a high throughput approach based on imaging flow cytometry. RBCs were classified based on the expression pattern of Lu/BCAM using the modulation feature that measures the intensity range and distribution of a fluorescent signal (see methods) (Figure 4C). Two main patterns were distinguished in this analysis: the “Low modulation” for weak intensity dispersed spots (Spots) and “High modulation” for strong intensity big patches (Patches) (Figure 4C, last panel). Both patterns were concomitantly present in all blood samples and all conditions. We compared the proportion of each pattern under oxidative and control conditions and found less RBCs with Spots and more with Patches in the presence of Cumene Hydroperoxide (Figure 4D, supplemental Figure S5.A), with no difference in Lu/BCAM global expression (Figure 4E), indicating that oxidation induces the formation of Lu/BCAM aggregates at the cell surface.

As expected, based on the confocal microscopy results, oxidation did not impact the proportions of ICAM-4 Spots and Patches subpopulations (Figure 4F, supplemental Figure S5.A) or its global expression at the RBC surface (Figure 4G).

Finally, we assessed Lu/BCAM distribution on SS LD and HD RBCs in which both the Spots and the Patches patterns were found. Similar to oxidized AA RBCs, the percentage of cells with the Patches pattern was higher in HD RBCs in comparison with LD RBCs, while the Spots pattern prevailed in the LD subpopulation (Figure 4H, supplemental Figure S5.B). As expected and already reported, Lu/BCAM expression was lower in HD than in LD RBCs (Figure 4I).

Less GPC sialylation on SS RBCs

Impact of sialic acid removal on Lu/BCAM membrane distribution

We have recently shown that Lu/BCAM can establish *cis*-interactions with glycophorin C (GPC) sialic acids at the RBC surface keeping it in a "locked" conformation impeding its interaction with laminin (32). To test if such interactions modulate the Lu/BCAM expression pattern, AA RBCs were treated with Neuraminidase (N'ase) in order to eliminate protein sialic acids, labeled with an anti-Lu/BCAM antibody and analyzed by imaging flow cytometry. We found that loss of sialic acids resulted in less Spots and more Patches RBCs (Figure 5A) with no impact on Lu/BCAM global expression level (Figure 5B), indicating that lateral interactions of Lu/BCAM with sialic acid residues impede its capacity to aggregate at the cell surface. Altogether, these results suggest that oxidation may trigger Lu/BCAM release from sialic acid lateral interactions leading to its aggregation and activated adhesive function.

Total sialylation and specific GPC sialylation levels

As HD RBCs showed higher percentages of cells with the Patches pattern and that treatment of AA RBCs with N'ase increases also the proportions of this sub-population, we hypothesized that increased HD RBC adhesion to laminin might result from aggregation of Lu/BCAM molecules subsequent to altered GPC sialylation. Using biotinylated lectins, we measured the sialic acid levels at the surface of RBCs from 9 AA and 9 SS blood samples by flow cytometry and found no significant difference between the two groups (Figure 5C). We performed the same analysis on 7 SCD fractionated blood samples and found less sialic acid at the surface of all HD RBCs when compared to LD RBCs (Figure 5D), suggesting that increased adhesion to laminin of HD RBCs might result from the partial loss of interaction between Lu/BCAM and GPC at the cell surface. To specifically address GPC sialylation levels, we used an antibody directed against sialylated forms of GPC. Flow cytometry analysis showed less GPC sialylation levels in HD than in LD RBCs (Figure 5E), while no significant difference was observed in total amounts of GPC at the cell surface as determined by flow cytometry using a sialic acid-independent anti-GPC antibody (Figure 5F). This result supported our hypothesis of increased HD RBC adhesion to laminin following altered *cis*-interactions of Lu/BCAM with GPC at the cell surface.

Discussion

Oxidative stress is an important feature of SCD and plays an important role in the pathophysiology of hemolysis, vaso-occlusion and ensuing organ damage. In this study we investigated the relationship between oxidative stress and adhesion of RBCs to laminin. We report altered protein *cis*-interactions at the surface of sickle dense RBCs that may account for the activation of RBC adhesion in the absence of signaling events and contribute to vaso-occlusion.

Using the microfluidic biomimetic chip, we confirm the importance of the mechanical parameter in the preferential trapping of HD RBCs at a single cell level, confirming the hypothesis of the 2-step model in which dense RBCs contribute to the obstruction of fine blood vessels because of reduced deformability (13). In addition, we show that HD RBCs adhere more firmly to laminin and are more resistant to shear stress than LD RBCs suggesting that they would also contribute to initiate VOCs *in vivo* by adhering to the vessel wall even at high shear stress. This difference is probably partly due to the increased rigidity of HD RBCs, as well as to the difference in cell shape between both subtypes, with a majority of very young and round reticulocytes in the LD fraction having a smaller contact surface with the capillary wall than HD RBCs that are flatter cells with a larger contact surface and a smaller section facing the flow after adhesion is initiated. This is supported by the presence of long cellular tethers and of big patches of Lu/BCAM on several adhering LD RBCs indicative of important membrane dynamics in this subpopulation, which is a characteristic of reticulocytes known to undergo skeletal and membrane remodeling during maturation (33, 34).

Several studies have investigated the dynamics and rheology of SS RBCs under flow conditions using microfluidic devices. Alapan *et al* assessed sickle RBC adhesion in fibronectin-coated microfluidic chips and observed significantly greater numbers of adhered non-deformable than deformable RBCs (35). Our study extends these findings by comparing

the adhesion of deformable and non-deformable RBCs within both the young and mature populations. As a matter of fact, fibronectin is the substrate of integrin $\alpha_4\beta_1$ that is expressed only in very young reticulocytes, restricting the analysis to a very small subpopulation of RBCs, while the laminin receptor Lu/BCAM is expressed on RBCs at all the maturation stages.

We show that oxidation can activate RBC adhesion to laminin by inducing post-translational modifications of Lu/BCAM that modify its distribution at the cell surface generating aggregates with high binding potential to laminin. This mechanism targets and abolishes Lu/BCAM *cis*-interaction with GPC at the cell surface (32) and seems to be specific for Lu/BCAM and to target GPC primarily, as another IgSF member, i.e. LW/ICAM-4, was not impacted by *in vitro* oxidation and did not show altered distribution at the surface of SS RBCs. Abnormal RBC adhesion to laminin was reported in several pathologies (15) with two triggering mechanisms including Lu/BCAM phosphorylation (17, 24, 27) and Lu/BCAM dissociation from the spectrin-based skeleton (25, 26, 36). Here, the oxidation-driven mechanism seems to be at the origin of increased adhesion of HD RBCs in the absence of Lu/BCAM phosphorylation and seems in line with the high adhesion levels of HD RBCs in the absence of responsiveness to cAMP inducers (28). Moreover, although abnormal actin oxidation has been reported in irreversibly sickled cells affecting cytoskeletal dynamics (37), in our study oxidation and the subsequent loss of interaction with GPC do not alter Lu/BCAM binding to the skeleton as we did not see a difference in Lu/BCAM Triton extractability between *in vitro* oxidized and non-oxidized AA RBCs (data not shown). This is supported by the unchanged mobility of Lu/BCAM at the surface of neuraminidase-treated RBCs as measured by fluorescence recovery after photobleaching (FRAP) assays (32). As a matter of fact, oxidation may impact the interactions of membrane proteins with the skeleton as it was

reported for Band 3 (38-41) but here Lu/BCAM activation seems to be triggered by modifications at the extracellular rather than the intracellular side.

During erythrocyte lifespan, sialic acid levels gradually decrease (42-44). The sialic acid levels were lower on HD than on LD RBCs for all blood samples, corroborating the finding that sialoglycoproteins are enriched in membranes of young reticulocytes (45) and indicating an accelerated aging-like phenotype between the two stages despite the very short lifespan of RBCs in SCD (46, 47). This suggests increased damage of the RBC surface in SCD, targeting the glycocalyx, probably mediated by high levels of oxidative stress effectors in the plasma including free hemoglobin (48).

Our study extends our recent findings on the novel mechanism activating Lu/BCAM-mediated RBC adhesion and suggests that this mechanism could be triggered by oxidative stress activating the adhesion of dense sickle RBCs in the absence of Lu/BCAM phosphorylation. It would be interesting to determine the impact of anti-oxidant drugs on this specific mechanism and to evaluate their potential of reducing or attenuating RBC adhesion in SCD.

Author contributions

MALI and SDL conducted experiments, acquired and analyzed data and wrote the manuscript; VB provided blood samples and discussed data; SC, SEH, AF, MD and SA conducted experiments, analyzed data and edited the manuscript; CLVK and FRL discussed data and edited the manuscript; OF, BLP, TK and RvB conducted experiments, discussed data and edited the manuscript; WEN designed research, analyzed data and wrote the manuscript.

Conflict of Interest Disclosures

The authors declare no conflict of interest.

References

1. Pauling L, Itano HA, Singer SJ, Wells IC. Sickle cell anemia, a molecular disease. Science. 1949;110(2865):543-548.
2. Piel FB, Steinberg MH, Rees DC. Sickle Cell Disease. N Engl J Med. 2017;376(16):1561-1573.
3. Ware RE, Montalembert MD, Tshilolo L, Abboud MR. Sickle cell disease. Lancet. 2017;6736(17):1-13.
4. Barabino GA, Platt MO, Kaul DK. Sickle Cell Biomechanics. Annu Rev Biomed Eng. 2010;12:345-367.
5. Connes P, Lamarre Y, Waltz X, et al. Haemolysis and abnormal haemorheology in sickle cell anaemia. Br J Haematol. 2014;165(4):564-572.
6. Stuart MJ, Nagel RL. Sickle-cell disease. Lancet. 2004;364(9442):1343-1360.
7. Hebbel RP. Beyond hemoglobin polymerization: the red blood cell membrane and sickle disease pathophysiology. Blood. 1991;77(2):214-237.
8. Hebbel RP. Adhesive interactions of sickle erythrocytes with endothelium. J Clin Invest. 1997;99(11):2561-2564.
9. Hebbel RP, Yamada O, Moldow CF, Jacob HS, White JG, Eaton JW. Abnormal adherence of sickle erythrocytes to cultured vascular endothelium. Possible mechanism for microvascular occlusion in sickle cell disease. J Clin Invest. 1980;65(1):154-160.
10. Cartron J, Elion J. Erythroid adhesion molecules in sickle cell disease : Effect of hydroxyurea. Transfus Clin Biol. 2008;15(1-2):39-50.
11. Kaul DK, Fabry ME. In vivo studies of sickle red blood cells. Microcirculation. 2004;11(2):153-165.
12. Kaul DK, Fabry ME, Nagel RL. Microvascular sites and characteristics of sickle cell adhesion to vascular endothelium in shear flow conditions: pathophysiological implications. Proc Natl Acad Sci U S A. 1989;86(9):3356-3360.
13. Kaul DK, Finnegan E, Barabino Ga. Sickle red cell-endothelium interactions. Microcirculation. 2009;16(1):97-111.

14. Kaul DK, Nagel RL. Sickle cell vasoocclusion: many issues and some answers. Experientia. 1993;49(1):5-15.

15. Colin Y, Le van Kim C, El Nemer W. Red cell adhesion in human diseases. Curr Opin Hematol. 2014;21(3):186-192.

16. El Nemer W, Gane P, Colin Y, et al. The Lutheran blood group glycoproteins, the erythroid receptors for laminin, are adhesion molecules. J Biol Chem. 1998;273(27):16686-16693.

17. Gauthier E, Wautier MP, Nemer WE, et al. Protein kinase a-dependent phosphorylation of lutheran/basal cell adhesion molecule glycoprotein regulates cell adhesion to laminin α5. J Biol Chem. 2005;280(34):30055-30062.

18. Telen MJ. Sickle cell anemia role of adhesion molecules and vascular endothelium in the pathogenesis of sickle cell disease. Hematology Am Soc Hematol Educ Program. 2007;84-90.

19. Udani M, Zen Q, Cottman M, et al. Basal cell adhesion molecule/lutheran protein: The receptor critical for sickle cell adhesion to laminin. J Clin Invest. 1998;101(11):2550-2558.

20. Zennadi R, Hines PC, De Castro LM, Cartron JP, Parise LV, Telen MJ. Epinephrine acts through erythroid signaling pathways to activate sickle cell adhesion to endothelium via LW-alphavbeta3 interactions. Blood. 2004;104(12):3774-3781.

21. Zennadi R, Moeller BJ, Whalen EJ, et al. Epinephrine-induced activation of LW-mediated sickle cell adhesion and vaso-occlusion in vivo. Blood. 2007;110(7):2708-2717.

22. Parsons SF, Mallinson G, Holmest CH, et al. The Lutheran blood group glycoprotein, another member of the immunoglobulin superfamily, is widely expressed in human tissues and is developmentally regulated in human liver. Blood. 1995;92(12):5496-500.

23. Rahuel BC, Kim CLV, Mattei MG, Cartron JP, Colin Y. Unique Gene Encodes Spliceoforms of the B-Cell Adhesion Molecule Cell Surface Glycoprotein of Epithelial Cancer and of the Lutheran Blood Group Glycoprotein. Blood. 1996;88(5):1865-1872.

24. De Grandis MD, Cambot M, Wautier M-p, Cassinat B, Chomienne C, Colin Y, et al. JAK2V617F activates Lu/BCAM-mediated red cell adhesion in polycythemia vera through an EpoR-independent Rap1/Akt pathway. Blood. 2007;121(4):658-66.

25. An X, Gauthier E, Zhang X, et al. Adhesive activity of Lu glycoproteins is regulated by interaction with spectrin. Blood. 2008;112(13):5212-5219.

26. Gauthier E, El W, Wautier MP, et al. Role of the interaction between Lu/BCAM and the spectrin-based membrane skeleton in the increased adhesion of hereditary spherocytosis red cells to laminin. Br J Haematol. 2009;148(3):456-465.

27. Bartolucci P, Chaar V, Picot J, et al. Decreased sickle red blood cell adhesion to laminin by hydroxyurea is associated with inhibition of Lu/BCAM protein phosphorylation. Blood. 2010;116(12):1-4.

28. Hines PC, Zen Q, Burney SN, et al. Novel epinephrine and cyclic AMP-mediated activation of BCAM/Lu-dependent sickle (SS) RBC adhesion. Blood. 2003;101(8):3281-3287.

29. McDonald JC, Whitesides GM. Poly (dimethylsiloxane) as a material for fabricating microfluidic devices. Acc Chem Res. 2002;35(7):491-499.

30. Schneider CA, Rasband WS, Eliceiri KW, Instrumentation C. NIH Image to ImageJ : 25 years of Image Analysis. Nat Methods. 2012;9(7):671-675.

31. Picot J, Ndour PA, Lefevre SD, et al. A biomimetic microfluidic chip to study the circulation and mechanical retention of red blood cells in the spleen. Am J Hematol. 2015;90(4):339-345.

32. Klei TRL, Back DZD, Asif PJ, et al. Glycophorin-C sialylation regulates Lu/BCAM adhesive capacity during erythrocyte aging. Blood. 2018;2(1):14-24.

33. Chasis JA, Prenant M, Leung A, Mohandas N. Membrane assembly and remodeling during reticulocyte maturation. Blood. 1989;74(3):1112-1120.

34. Mohandas N, Groner W. Cell membrane and volume changes during red cell development and aging. Ann N Y Acad Sci. 1989;554:217-224.

35. Alapan Y, Matsuyama Y, Little JA, Gurkan UA. Dynamic deformability of sickle red blood cells in microphysiological flow. Technology (Singap World Sci). 2016;4(2):71-79.

36. Wandersee NJ, Olson SC, Holzhauer SL, Hoffmann RG, Barker JE, Hillery CA. Increased erythrocyte adhesion in mice and humans with hereditary spherocytosis and hereditary elliptocytosis. Blood. 2004;103(2):710-717.

37. Shartava A, Monteiro CA, Bencsath FA, et al. A posttranslational modification of beta-actin contributes to the slow dissociation of the spectrin-protein 4.1-actin complex of irreversibly sickled cells. J Cell Biol. 1995;128(5):805-818.

38. Arashiki N, Kimata N, Manno S, Mohandas N, Takakuwa Y. Membrane peroxidation and methemoglobin formation are both necessary for Band 3 clustering: mechanistic insights into human erythrocyte senescence. Biochemistry. 2013;52(34):5760-5769.

39. Mannu F, Arese P, Cappellini MD, et al. Role of hemichrome binding to erythrocyte membrane in the generation of Band-3 alterations in B-Thalassemia intermedia erythtrocytes. Blood. 1995;86(5):2014-2020.

40. Pantaleo A, Giribaldi G, Mannu F, Arese P, Turrini F. Naturally occurring anti-band 3 antibodies and red blood cell removal under physiological and pathological conditions. Autoimm Rev. 2008;7(6):457-462.

41. Noomuna P, Risinger M, Zhou S, et al. Inhibition of Band 3 tyrosine phosphorylation: a new mechanism for treatment of sickle cell disease. Br J Haematol. 2020 Apr 28. [Epub ahead of print]

42. Hadengue AL, Del-pino M, Simon A, Levenson J. Erythrocyte disaggregation shear stress, sialic acid, and cell aging in humans. Hypertension. 1998;32(2):324-330.

43. Huang Y-x, Tuo W-w, Wang D, Kang L-l, Chen X-y, Luo M. Restoring the youth of aged red blood cells and extending their lifespan in circulation by remodelling membrane sialic acid. J Cell Mol Med. 2016;20(2):294-301.

44. Shinozuka T. Changes in human red blood cells during aging in vivo. Kelo J Med. 1994;43(3):155-163.

45. Skutelsky E, Farquhar M. Variations in distribution of Con A receptor sites and anionic groups during red blood cell differentiation in the rat. J Cell Biol. 1976;71(1):218-231.
46. Franco RS, Lohmann J, Silberstein EB, Mayfield-pratt G, Palascak M, Nemeth TA. Time-dependent Changes in the Density and Hemoglobin F Content of Biotin-Labeled Sickle Cells. J Clin Invest. 1998;101(12):2730-2740.
47. Quinn CT, Smith EP, Arbabi S, et al. Biochemical surrogate markers of hemolysis do not correlate with directly measured erythrocyte survival in sickle cell anemia. Am J Hematol. 2016;91(12):1195-1201.
48. Rifkind JM, Mohanty JG, Nagababu E. The pathophysiology of extracellular hemoglobin associated with enhanced oxidative reactions. Front Physiol. 2015;5:500.

Figure legends

Figure 1. Analysis of RBC deformability using a microfluidic biomimetic chip. (A) *Left panel*: The microfluidic device comprises eight filtering units arranged in parallel. *Right panel*: Each filtering unit is 5 µm-high and has a U shape composed of a series of 15 µm pillars separated by 5 µm slits, with two 10 µm-wide side channels. Inside the U shape, 4 rows are disposed in parallel with decreasing slit width (10, 8, 7 and 6 µm). (B) Microscopy image showing SS RBCs (green) and AA RBCs (red) trapped into the filtering unit slits. (C) Retention percentage of AA and SS RBCs in the 5 µm slits. Mann-Whitney test, ***P < 0.0001 (D) Microscopy image showing LD RBCs (green) and HD RBCs (red) trapped into the peripheral 5 µm slits of the filtering unit. The majority of the other cells are in motion in the space separating two consecutive walls (E) Retention percentage of LD and HD RBCs in the peripheral 5 µm slits. Wilcoxon test, *P < 0.05. In the graphs C and E the data is expressed as the percentage of cells from each RBC type trapped into the 5 µm slits, considering the total number of cells trapped into the 5 µm slits as 100% (n=7).

Figure 2. Adhesion to laminin and shear stress resistance of SS RBC subpopulations. (A). Adhesion assays under flow conditions were done by perfusing LD and HD RBCs from 7 SCD patients through a biochip coated with Laminin 521. The amount of RBCs, of each subpopulation and each blood sample, attached at 1 dyn/cm^2 was considered as 100% and used to determine the percentage of attached RBCs at increasing shear stress, as indicated on the *x*-axis. The percentage of HD RBCs (■) attached to laminin was higher than the percentage of LD RBCs (▲). Paired *t* test, **P < 0.005. (B) Tracking of mobile cells during a flow adhesion assay for LD (*upper panel*) and HD (*lower panel*) RBCs at 3 dyn/cm². (C) Computational treatment of brightfield images of the same field to identify immobile cells between 2 and 3 dyn/cm² during a flow adhesion assay. Overlaid image (*bottom panel*)

revealing immobile cells in dark grey and mobile cells in light grey (D) Quantification of immobile cells for LD (▲) and HD (■) RBCs from blood samples of 4 SCD patients. Results are expressed as percentage of immobile cells between two consecutive shear stress values. Paired *t* test, **P* < 0.05. (E) Representative images of Lu/BCAM detected by immunofluorescence as well as tether length of LD and HD RBCs in a flow adhesion assay at high shear stress (7 dyn/cm²). (F) Percentage of tether-containing cells in each RBC subpopulation at 7 dyn/cm². Paired *t* test, **P* < 0.05. (G) Tether length in LD and HD RBCs. Mann-Whitney test, *****P* < 0.0001.

Figure 3. Effect of *in vitro* oxidation on AA RBC adhesion to laminin. (A) *Left panel*: Typical microscopy images of non-oxidized and Cumene Hydroperoxide-oxidized AA RBCs adhering to Laminin 521 at 3 dyn/cm^2. *Right panel*: Quantification of cell adhesion showing the mean number of adherent RBCs/mm^2 in 7 oxidized and non-oxidized AA RBC samples at 3 dyn/cm^2. Wilcoxon test, **P* < 0.05. (B) Flow cytometry analysis of Lu/BCAM expression at the RBC surface expressed as percentage of Lu/BCAM-positive RBCs (*left panel*) and mean fluorescence intensity (MFI) of these RBCs (*right panel*) under non-oxidized (PBS) and oxidized conditions (Cumene). No significant differences were observed, Wilcoxon test, *P* = 0.0714.

Figure 4. Expression pattern of Lu/BCAM and ICAM-4 on RBCs by confocal microscopy and imaging flow cytometry. Confocal microscopy images of RBCs expressing (A) Lu/BCAM and (B) ICAM-4 under non-oxidized and oxidized conditions. (C) Imaging flow cytometry analysis steps of Lu/BCAM expression on the RBC surface. After gating the single cells, gating is set on RBCs facing the camera (circular cells), then on those expressing Lu/BCAM. In the final step a modulation feature is applied to measure the intensity range and

distribution of Lu/BCAM, and define two main patterns: Low Modulation (Spots) and High Modulation (Patches). (D) Percentage of Lu/BCAM-positive RBCs with Spots pattern *(left)* and Patches pattern *(right)* (n=10). Wilcoxon test,$^{**}P < 0.01$. (E) Representative flow cytometry plots of Lu/BCAM expression in a non-oxidized (PBS) and oxidized (Cumene Hydroperoxide) AA RBC sample. (F) Percentage of ICAM-4-positive RBCs with Spots pattern *(left)* and Patches pattern *(right)* (n=8). Wilcoxon test, $P = 0.8125$ and 0.3828. (G) Representative flow cytometry plots of ICAM-4 expression in a non-oxidized (PBS) and oxidized (Cumene Hydroperoxide) AA RBC sample. (H) Percentage of Lu/BCAM-positive RBCs with Spots pattern (*left*) and Patches pattern (*right*) in LD and HD SS RBCs (n=8); Wilcoxon test, $^{**}P<0.01$, $^{*}P < 0.05$. (I) Representative flow cytometry plots of Lu/BCAM expression in LD and HD RBCs from one SS blood sample.

Figure 5. Sialic acid levels, GPC sialylation and Lu/BCAM distribution in AA and SS RBCs. (A) Impact of neuraminidase (N'ase) treatment on Lu/BCAM Spots and Patches patterns on AA RBCs. Wilcoxon test, $^{*}P < 0.05$. (B) Representative flow cytometry plots of Lu/BCAM expression in RBCs treated or not with neuraminidase. (C) *Left panel*: Sialic acid levels expressed as mean fluorescence intensity (MFI) on the RBC surface of 11 SS and 9 AA samples. No significant difference was found between both groups. Mann-Whitney test, $P = 0.224$. *Right panel*: Representative flow cytometry plots of sialic acid distribution on one AA and one SS RBC samples. (D) *Left panel*: Sialic acid levels expressed as mean fluorescence intensity (MFI) on the RBC surface of 8 LD and HD samples. Wilcoxon test, $^{**}P < 0.01$. *Right panel*: Representative flow cytometry plots of sialic acid distribution on LD and HD RBCs from the same SS blood sample. (E) *Left panel*: GPC sialylation levels expressed as mean fluorescence intensity (MFI) on the RBC surface of 8 LD and HD samples. Wilcoxon test, $^{*}P < 0.05$. *Right panel*: Representative flow cytometry plots of silalylated GPC on LD

and HD RBCs from the same SS blood sample. (F) *Left panel*: GPC expression represented as mean fluorescence intensity (MFI) on the RBC surface of 8 LD and HD samples. No significant differences were observed. Wilcoxon test, $P = 0.64$. *Right panel*: Representative flow cytometry plots of GPC expression on LD and HD RBCs from the same SS blood sample.

Figure 1

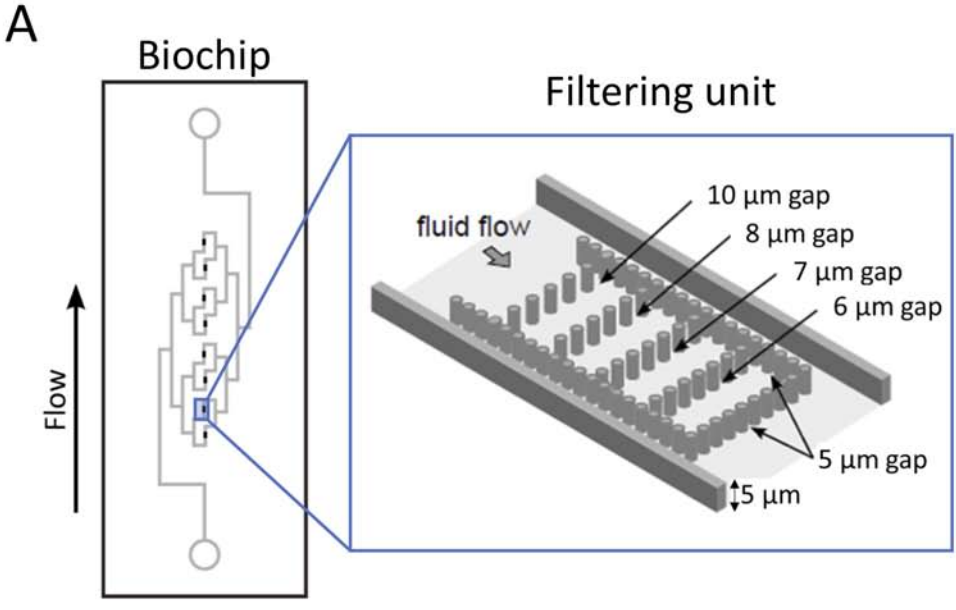
A
Biochip
Filtering unit
Flow
fluid flow
10 μm gap
8 μm gap
7 μm gap
6 μm gap
5 μm gap
5 μm

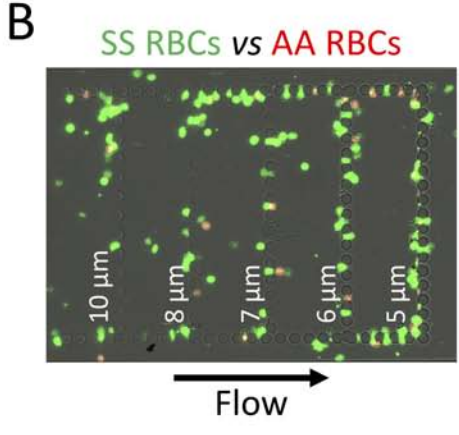
B
SS RBCs vs AA RBCs
10 μm
8 μm
7 μm
6 μm
5 μm
Flow

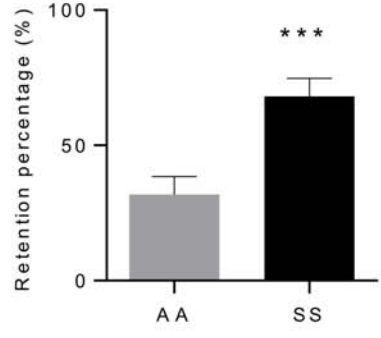
C
Retention percentage (%)
100
50
0
***
AA
SS

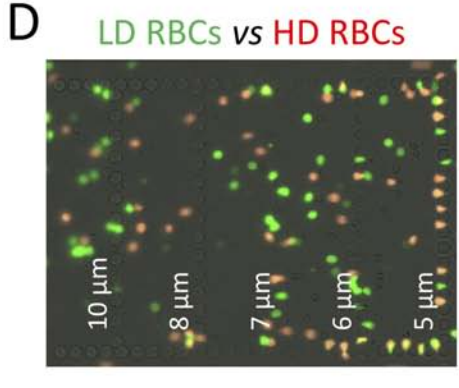
D
LD RBCs vs HD RBCs
10 μm
8 μm
7 μm
6 μm
5 μm

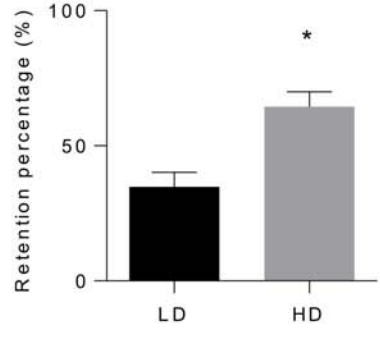
E
Retention percentage (%)
100
50
0
*
LD
HD

Figure 2

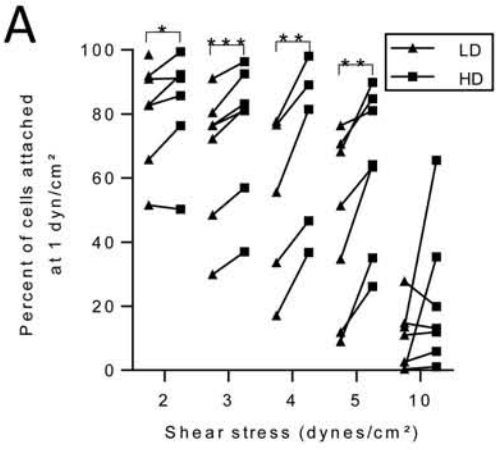
A
Percent of cells attached at 1 dyn/cm²
Shear stress (dynes/cm²)
LD
HD
*
***
**
**

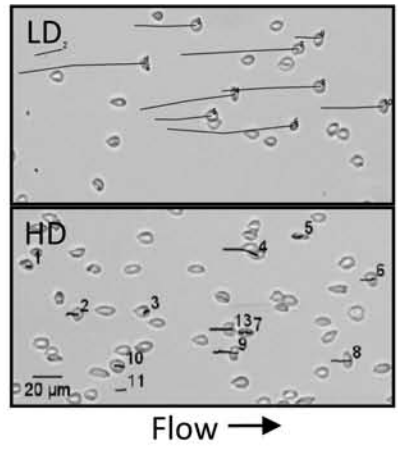
B
LD
HD
20 µm
Flow

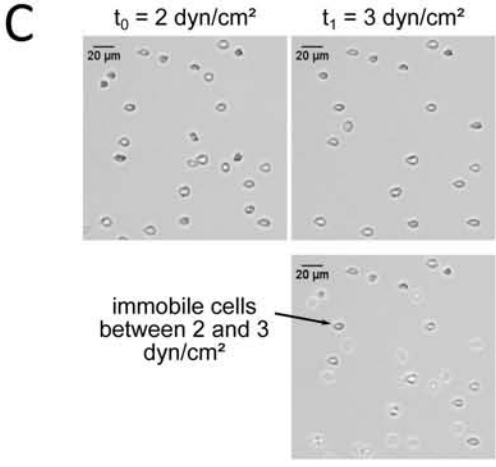
C
t0 = 2 dyn/cm²
t1 = 3 dyn/cm²
20 µm
immobile cells between 2 and 3 dyn/cm²

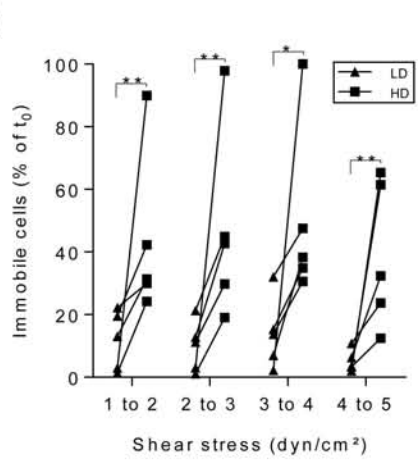
D
Immobile cells (% of t0)
LD
HD
1 to 2
2 to 3
3 to 4
4 to 5
Shear stress (dyn/cm²)

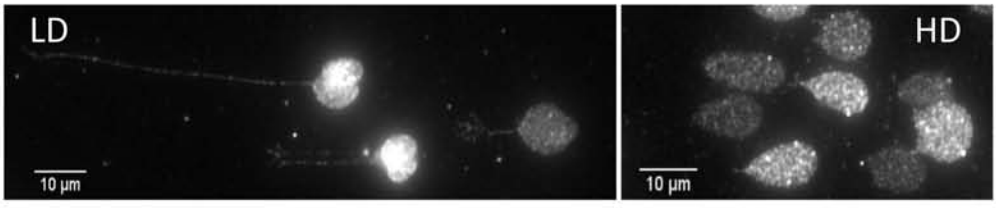
E
LD
HD
10 µm
10 µm

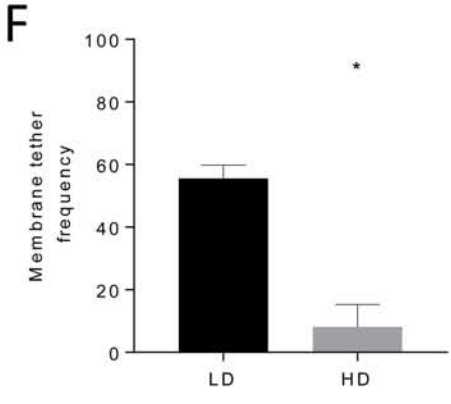
F
Membrane tether frequency
*
LD
HD

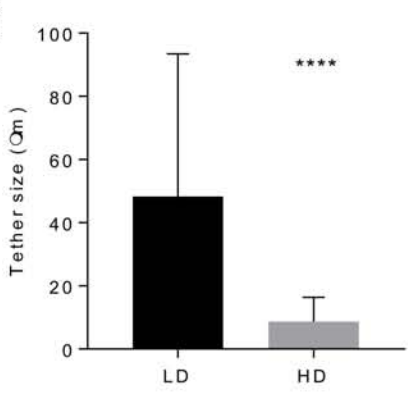
G
Tether size (Qm)
****
LD
HD

Figure 3

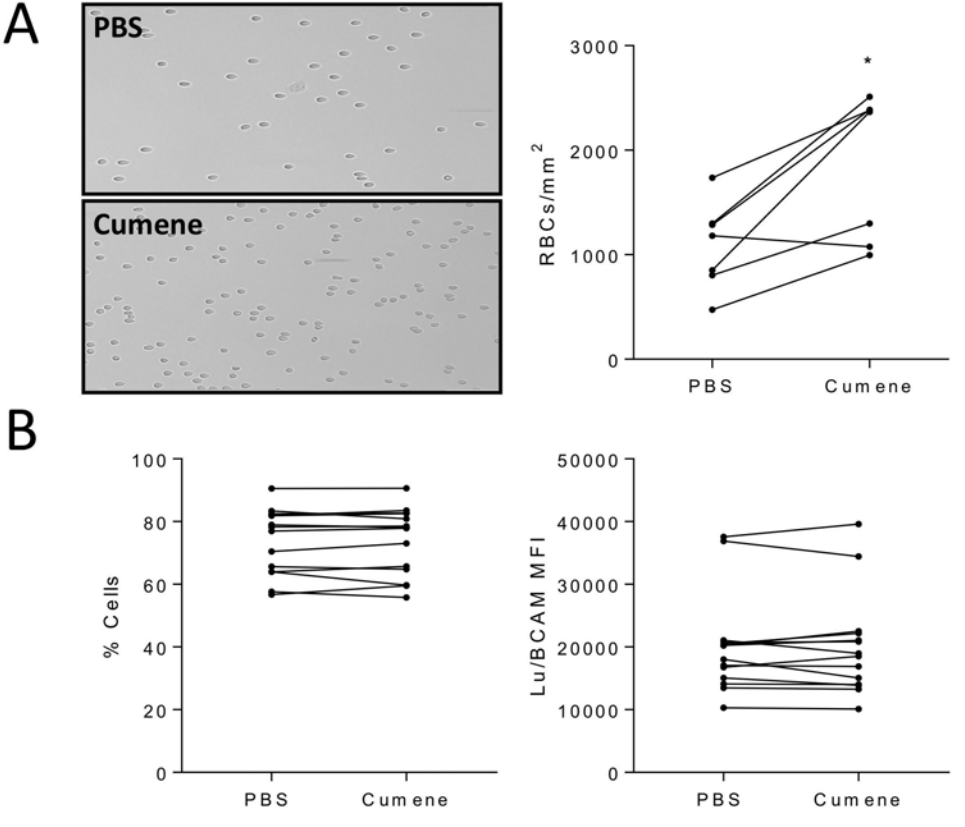
A
PBS
Cumene
3000
2000
1000
0
RBCs/mm2
*
PBS
Cumene
B
100
80
60
40
20
0
% Cells
PBS
Cumene
50000
40000
30000
20000
10000
0
Lu/BCAM MFI
PBS
Cumene

Figure 4

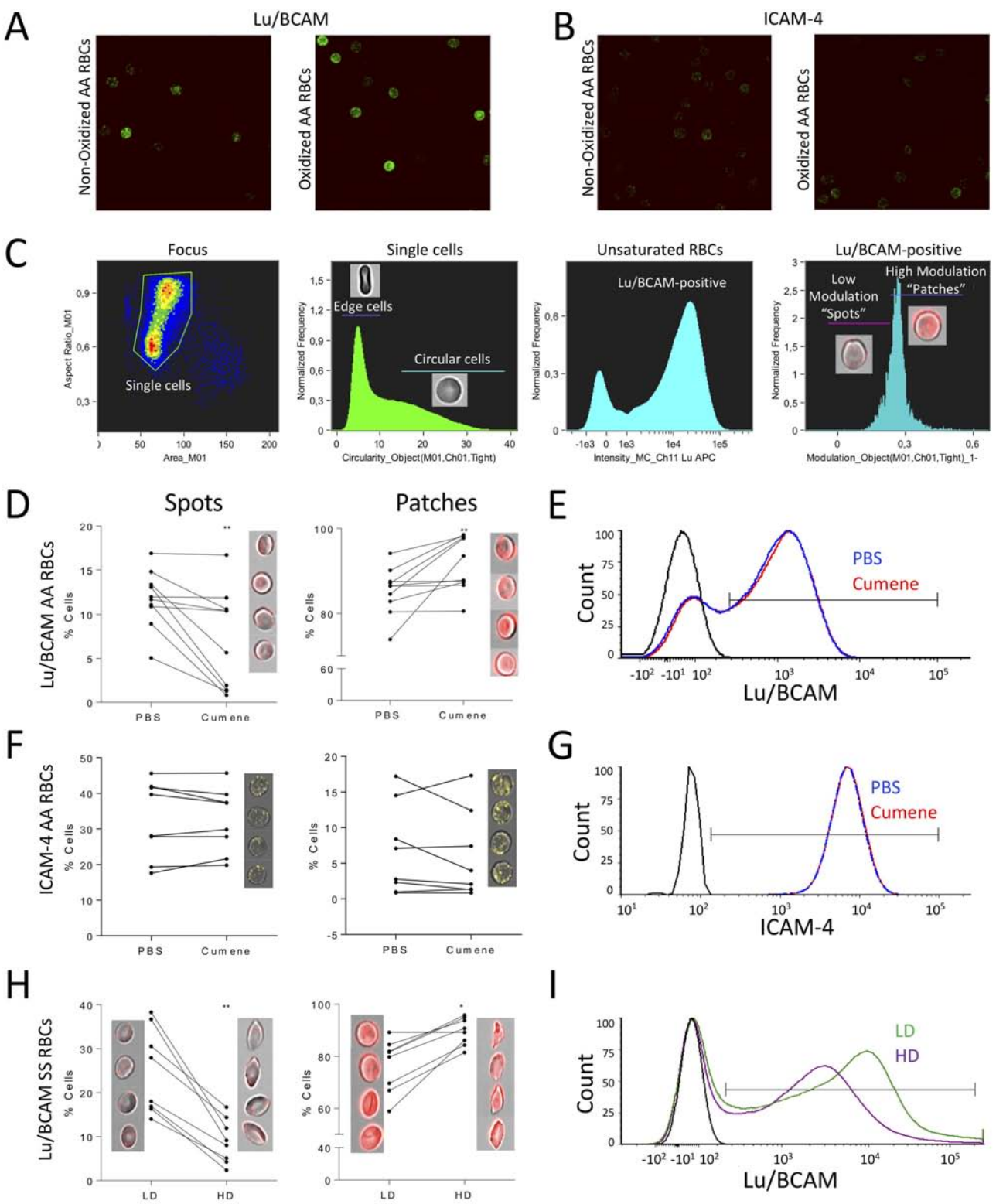
A
Lu/BCAM
Non-Oxidized AA RBCs
Oxidized AA RBCs
B
ICAM-4
Non-Oxidized AA RBCs
Oxidized AA RBCs
C
Focus
Aspect Ratio_M01
Single cells
Area_M01
Single cells
Edge cells
Circular cells
Normalized Frequency
Circularity_Object(M01,Ch01,Tight)
Unsaturated RBCs
Lu/BCAM-positive
Normalized Frequency
Intensity_MC_Ch11 Lu APC
Lu/BCAM-positive
Low Modulation "Spots"
High Modulation "Patches"
Normalized Frequency
Modulation_Object(M01,Ch01,Tight)_1-
D
Spots
Patches
Lu/BCAM AA RBCs
% Cells
PBS
Cumene
E
Count
PBS
Cumene
Lu/BCAM
F
ICAM-4 AA RBCs
% Cells
PBS
Cumene
G
Count
PBS
Cumene
ICAM-4
H
Lu/BCAM SS RBCs
% Cells
LD
HD
I
Count
LD
HD
Lu/BCAM

Figure 5

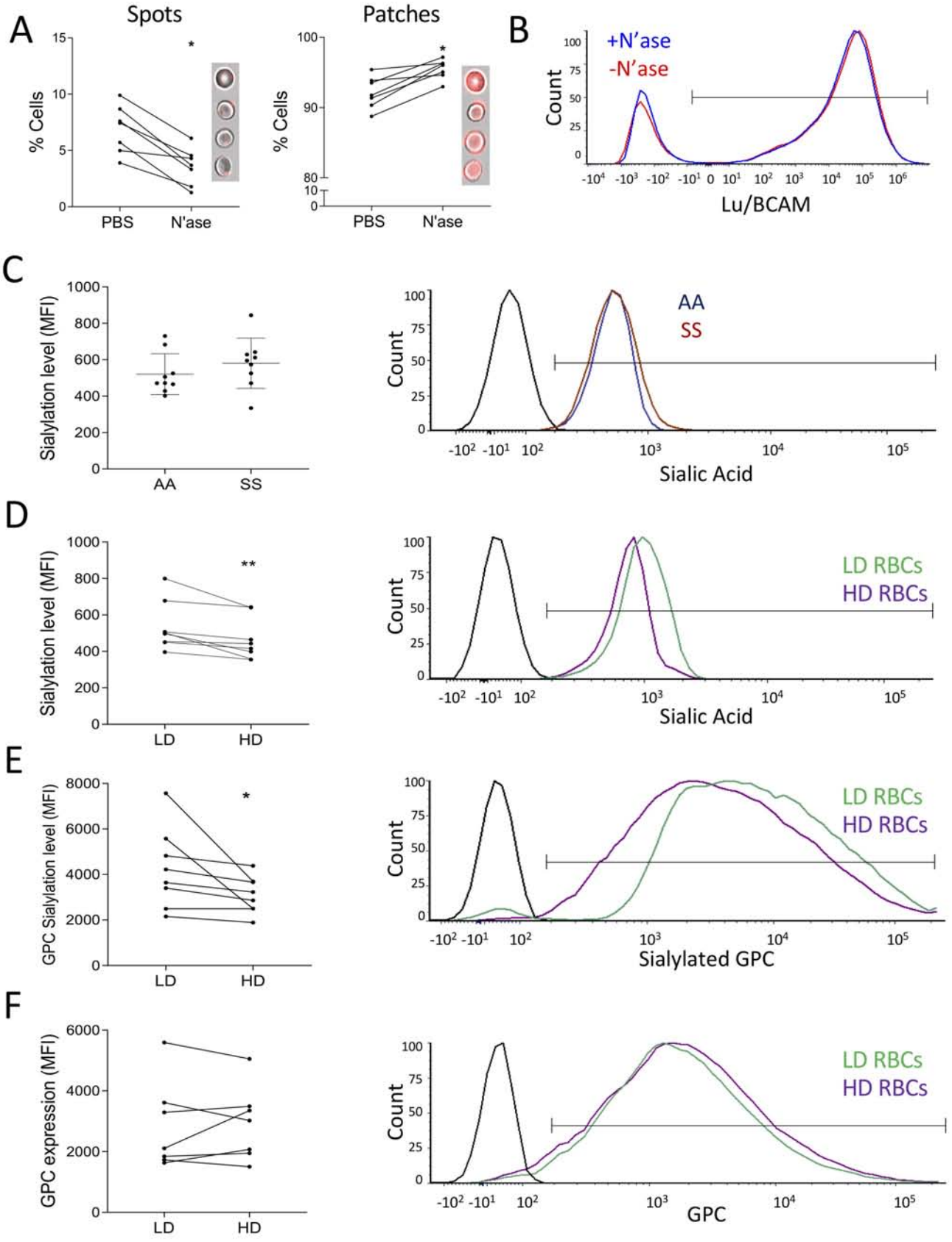
A
Spots
Patches
% Cells
PBS
N'ase
B
+N'ase
-N'ase
Count
Lu/BCAM
C
Sialylation level (MFI)
AA
SS
Sialic Acid
D
LD
HD
LD RBCs
HD RBCs
E
GPC Sialylation level (MFI)
Sialylated GPC
F
GPC expression (MFI)
GPC

Supplemental Figure S1

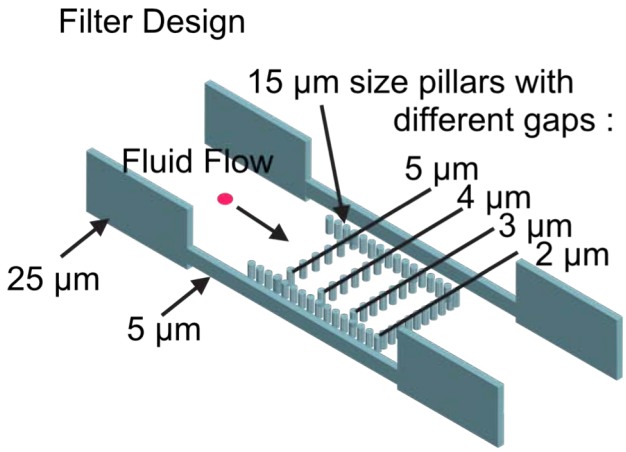

Supplemental Figure S1. Microfluidic biomimetic chip. One of the 8 filtering units of the microfluidic device. The filtering unit is 5 µm-high and has a U shape composed of a series of 15 µm pillars separated by 2 µm slits, with two 10 µm-wide side channels. Inside the U shape, 4 rows are disposed in parallel with decreasing slit width (5, 4, 3 and 2 µm).

Supplemental Figure S2

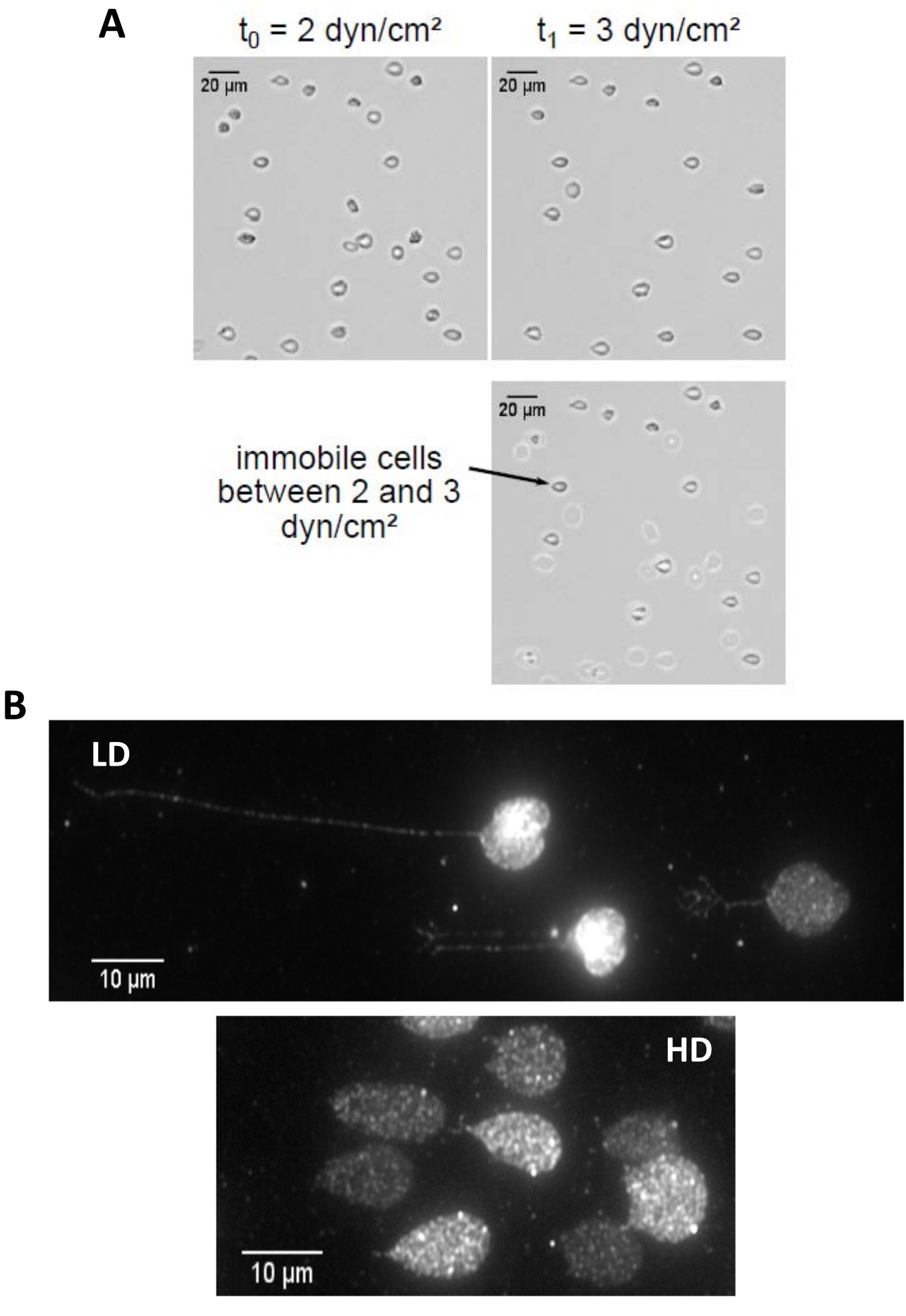

Supplemental Figure S2. Enlarged images from (A) Figure 2C and (B) Figure 2E.

Supplemental Figure S3

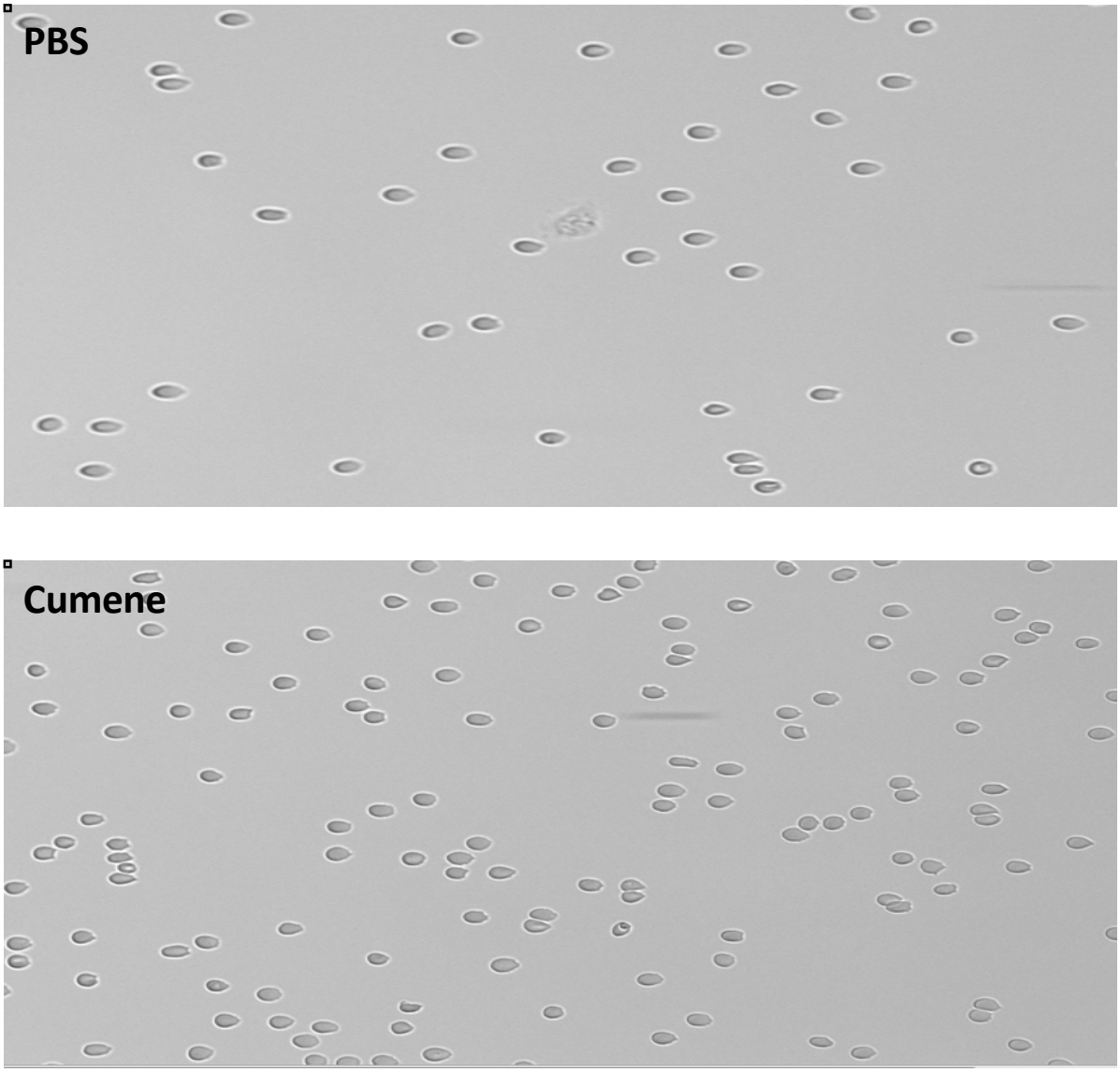

Supplemental Figure S3. Enlarged images from Figure 3A.

Supplemental Figure S4

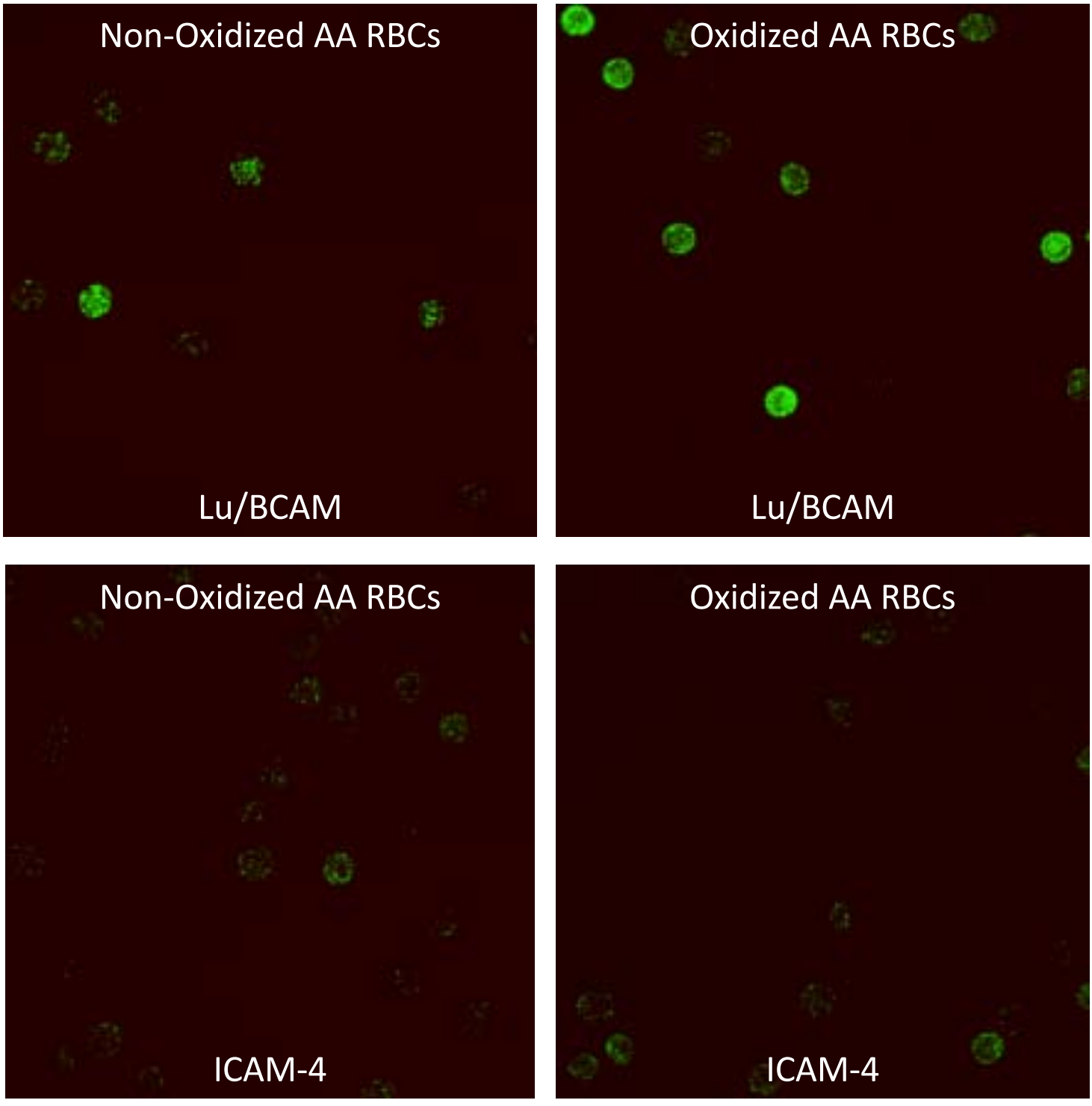

Supplemental Figure S4. Enlarged images from Figure 4A.

Supplemental Figure S5

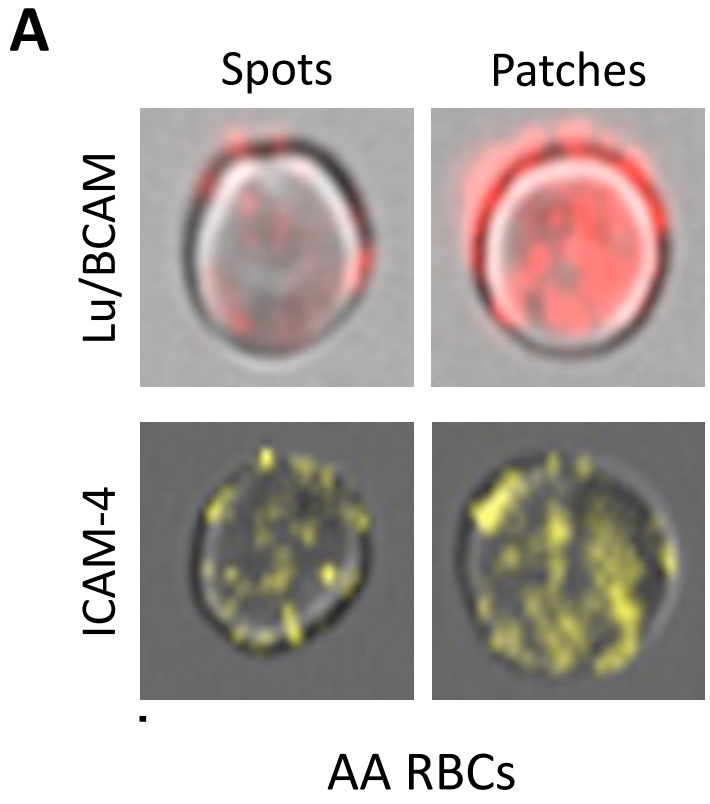

Supplemental Figure S5. Enlarged images from Figure 4 showing typical Lu/BCAM and ICAM-4 staining on (A) AA and (B) SS RBCs.

Video legend

Video 1: Adhesion to laminin 521 of sickle red blood cells (RBCs) from the low density (LD, top panel) and high density (HD, bottom panel) fractions (shear stress: 3 dyn/cm^2). HD RBCs adhere firmly to laminin while LD RBCs show a dual cellular behavior, with firm adhesion and rolling. The rolling LD RBCs are most probably young reticulocytes, as reflected by their round, multilobar morphology.